Journal of the European Ceramic Society 17 (1997) 1707–1713

PII: S0955-2219(97)00037-X
0955-2219/97/$17.00

Finite-Element Simulation of the Die Pressing and Sintering of a Ceramic Component

H. Zipse

Fraunhofer-Institut für Werkstoffmechanik, Wöhlerstraße 11, 79108 Freiburg, Germany

(Received 13 September 1996; revised version received 14 February 1997; accepted 17 February 1997)

Abstract

The industrial production of ceramic components via the powder route often leads to severe shape distortions of the sintered parts caused by friction effects during pressing. Computation of the geometry of the part after sintering helps the manufacturer to reduce these by modifying the pressing tools, thus avoiding expensive hard machining of each part. In the present paper, the results of a finite-element analysis of the process steps uniaxial dry pressing of a cylinder and sintering after green machining are reported. High density gradients after pressing are calculated near the die wall. The sintering simulation predicts a severe deformation of the dense cylinder and reveals the beneficial effect of removing regions of non-uniform density by green machining. The final shapes of simulated and sintered geometries are in good agreement. © *1997 Elsevier Science Limited.*

1 Introduction

For most ceramic parts, the fabrication via the powder route is well established in industry, mainly due to the relatively low cost for this kind of process. It often comprises uniaxial compaction of the ceramic powder in a die with subsequent machining of the green part. The following sintering procedure normally yields a ceramic part of nearly full (theoretical) density.

The demands on the processing technology are increasing because the geometries of the ceramic components are getting more and more complex and strict requirements concerning the shape tolerances of the sintered part have to be met by the manufacturer. Since hard machining of the sintered ceramic is expensive, one of the main goals in the industrial production process is the optimization of the processing route with respect to the geometry of the as-sintered part.

An empirical optimization is usually carried out by iteratively modifying the movement of the punches and changing the pressing tool and the die. This often involves many iteration loops and is therefore not only a tedious and expensive method but also makes delivery deadlines hard to meet for a newly designed product.

Here, a helpful tool is the finite-element method, which allows to simulate the processing steps die pressing and sintering if a constitutive model for the mechanical response of the material is available. Then, by evaluating the calculated final shapes of the parts, an optimization of cost and quality in the manufacture of technical ceramics becomes possible.

2 Die pressing

2.1 A model for powder compaction

Models for powder compaction usually describe the agglomerates as ideally plastic spheres with unlimited[1] or limited[2] cohesion between the particles. More recently, Fleck[3] found solutions for the yield surfaces in the case of an anisotropic distribution of grain contacts. Finite-element simulations of powder pressing[4] are often based on models developed originally for mineral materials such as soils and clays, some of which are implemented in general purpose finite-element programs (e.g. ABAQUS® or ADINA®). Bortzmeyer[5] uses a straight line cap model with non-associated flow in the cap region to simulate the densification behavior of zirconia powder. Nakagawa and Nohara,[6] on the other hand, model the cold isostatic pressing of alumina powder using constitutive equations for a porous visco-plastic material. In both cases, there is a fair correspondence between predicted and measured behaviour of the powder.

The pressing simulation presented in this paper uses the Drucker–Prager–Cap model for the

description of the flow behaviour, a materials option of the ABAQUS program package. The yield surface of this model consists of a linear slope describing failure under shear stresses with superimposed hydrostatic pressure, and an elliptical cap forming the boundary of the yield surface in direction of the hydrostatic axis, (Fig. 1). The cap yield surface is given by[7]

$$\Phi = \sqrt{(p-p_a)^2 + \left(\frac{Rt}{1+\alpha-\alpha/\cos\beta}\right)^2} - R(d + p_a \tan\beta) = 0 \quad (1)$$

where p is the hydrostatic stress, and t is a combination of the second and the third stress invariant. It coincides with the second invariant if the third invariant is neglected. tan β is the slope of the shear failure line, d is a parameter describing the amount of cohesion between the particles, R describes the shape of the cap, and α describes a transition surface between cap and failure line; p_b is a hardening parameter, and p_a is given by

$$p_a = \frac{p_b - R_d}{R\tan\beta + 1} \quad (2)$$

2.2 Determination of parameters

The yield function, eqn (1), is defined by several parameters, not all of them accessible by simple uniaxial pressing experiments. The parameters α, β, d, and R describe the shape of the yield surface and can only be measured by means of an instrumented triaxial pressing equipment which is not available yet at the author's institution. Therefore, estimated values are used. $\beta \approx 65°$ is found by comparison with a micromechanical model similar to Fleck's.[2] The values of the cohesion parameter and of the transition parameter are irrelevant for the uniaxial compaction process and are arbitrarily given the small values of $d = 0{\cdot}1$ MPa and $\alpha = 0{\cdot}1$. The shape parameter R can be inferred from measured ratios of radial to axial pressure, σ_r/σ_z, during die compaction.[8] Experimental results for that ratio are available for metal powders[9] and for hard metal powders.[10] The reported value for a hard metal powder is $\sigma_r/\sigma_z = 0{\cdot}46$. This corresponds to $R = 0{\cdot}6$. For metal powders, the ratio depends on the pressure and tends to be lower than 0·46. A value of $\sigma_r/\sigma_z = 0{\cdot}4$ was considered to be a reasonable average of the available data corresponding to $R = 0{\cdot}5$ which was chosen for the simulation.

The hardening curve describes the inflation of the yield surface for increasing volumetric strain. It is defined by the evolution of the hardening parameter p_b (Fig. 1) which can be measured in uniaxial die pressing experiments. For die compaction, p_b is given by

$$p_b + \frac{-(1 + R\tan\beta)\sigma_z}{1 + R\tan\beta\sqrt{1 + \left(\frac{2A}{3R}\right)^2}} \approx -0{\cdot}7864 \cdot \sigma_z \quad (3)$$

where σ_z is the axial compaction pressure. A is given by $A = 1 + \alpha - \alpha/\cos\beta$.

Experiments are performed using an Al_2O_3 dispersion powder containing 10 vol% of ZrO_2. It has an average grain size of 1 μm and an agglomerate size in the range of 20 to 280 μm. (Manufacturer FRIATEC AG, Frialit-Degussit, Mannheim, Germany.) The experimentally obtained force-displacement curve of the die pressing can be transformed into the $p_b - \varepsilon_{vol}$ curve of Fig. 2, and this hardening curve can be inserted into the ABAQUS input code. The model for pressing is thus identified.

For a simulation of the friction behaviour of the powder at the punches and die walls, the coefficient of friction was measured in a simple device. Two

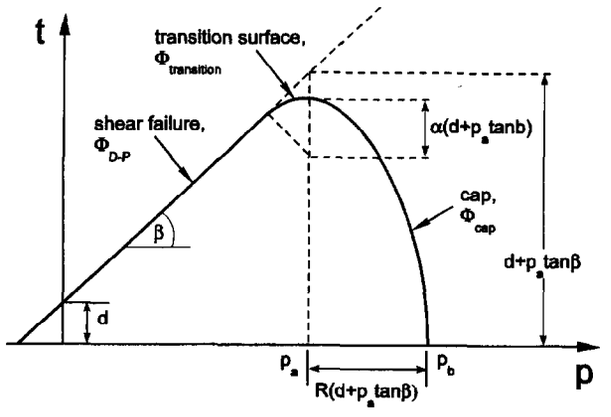

Fig. 1. Yield function of the Drucker–Prager Cap model in the plane of second stress invariant and pressure.

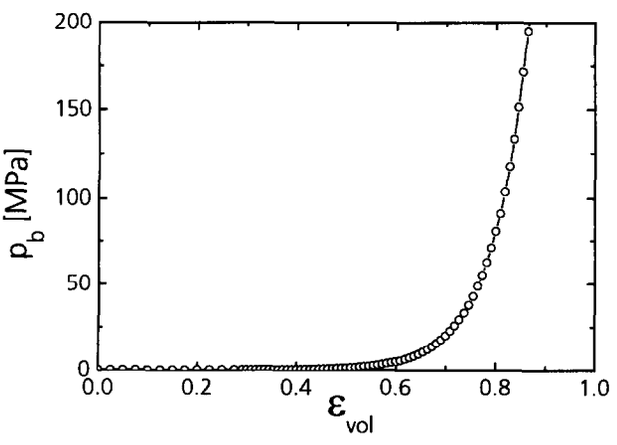

Fig. 2. Measured hardening curve $p_b(\varepsilon_{vol})$ of the investigated powder.

discs of green material were pressed against a rod of tool steel corresponding to the die material. The normal pressure was chosen to be of the same order of magnitude as the maximum radial stress acting on the die wall during dry pressing of the cylinder ($\sigma_N = 50$ MPa). The force to draw the rod with constant velocity divided by the normal force acting through the green discs yielded an average friction coefficient of $\mu = 0{\cdot}23$ for the investigated powder. μ is assumed to be constant during the pressing procedure.

2.3 Finite-element simulation of the die pressing

The part to be simulated is a component of a ceramic sensor used with chemically aggressive and abrasive media. The following investigation was realized in close co-operation with the manufacturer (FRIATEC AG, Mannheim, Germany). The sensor is made from the powder described above by uniaxial dry pressing of a full cylinder in a symmetrical double-acting press. Subsequent machining of the green cylinder includes material removal from the walls by outer turning and drilling of a conical hole in the axial direction. Figure 3 shows a photography of the part.

The values for the tap and the green densities, together with the dimensions of height and diameter of the green cylinder, allow the calculation of the powder volume before pressing and the stroke of the punches. Sliding contact between the die wall and the powder as well as between the punch and the powder is described by classical Coulomb friction. Punch and die wall are supposed to be rigid bodies. For reasons of symmetry, it is sufficient to simulate only one quadrant of an axial cut through the cylinder axis, (see Fig. 4). All the simulations presented in this paper were carried out with ABAQUS operating on an IBM AIX 3 RISC/6000 workstation.

The distorted mesh in Fig. 4 shows that the powder being pushed by the punch from above slides along the die wall, resulting in tangential forces on the wall. This results in a higher density in the vicinity of the corner between die wall and punch and a lower density in the centre plane near the die wall. The resulting density distribution is shown in Fig. 5.

A quantitative evaluation of the density distribution yields large density gradients near the die wall for both the upper surface of the cylinder and the centre plane (Fig. 6). High density gradients in the green body can lead to distortions, residual stresses, and even cracking of the sintered part. As a rule of thumb, only density gradients not exceeding 1% mm^{-1} can be tolerated by the manufacturer. This means that the regions of high gradients near the cylinder surface (shaded area in Fig. 6) should be removed by green machining.

3 Green machining

Green machining is technologically demanding due to the low strength and the brittleness of the green body resulting in difficulties in handling, gripping, and machining. However, the simulation of the process on the computer is straightforward as long as only the shape and the density before and after machining is of interest. Assuming that the material removal does not influence the spatial density distribution, it suffices to project the calculated density distribution of the green body on the geometry of the machined part. The result is shown in Fig. 7. It is obvious that the regions of high density gradients have been removed and a more homogeneous density distribution is achieved. Shape distortions after sintering and the risk of cracks are reduced.

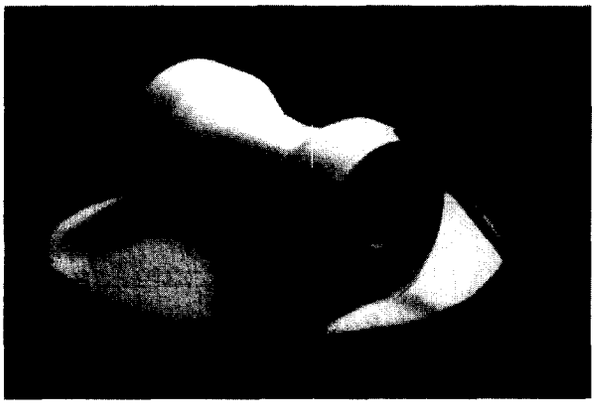

Fig. 3. Photography of the green part after machining.

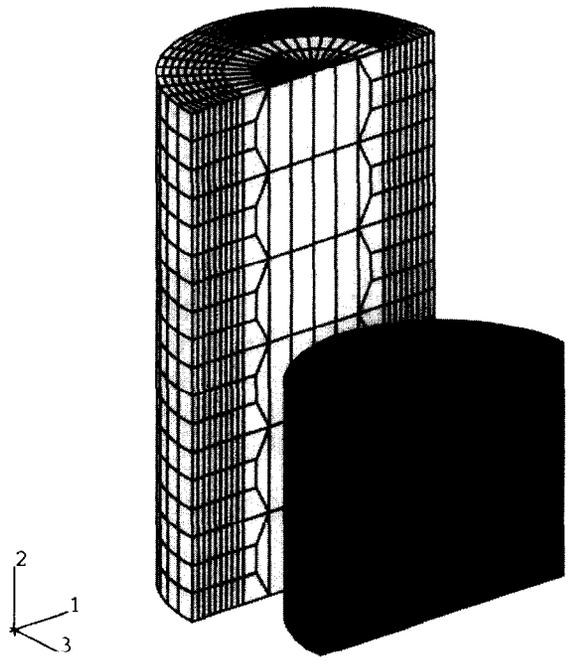

Fig. 4. Finite-element mesh before and after pressing. The upper half of an axial cut through the cylinder centre is shown.

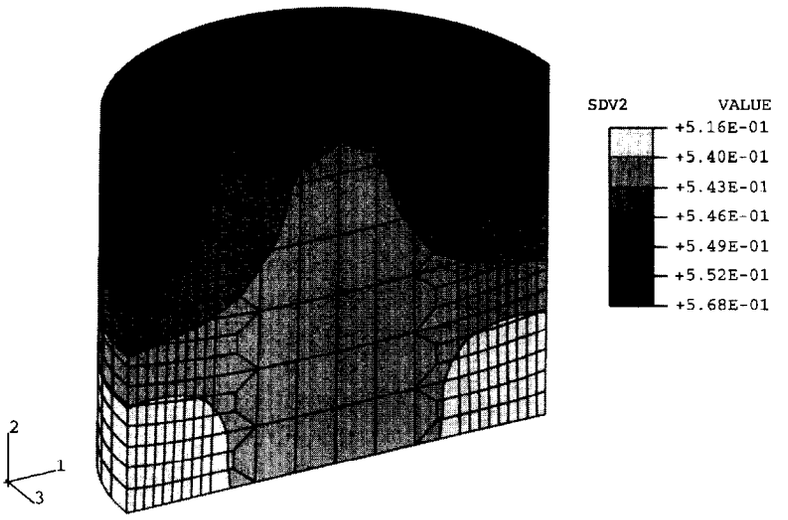

Fig. 5. Distribution of the relative density in the upper half of an axial cut through the green cylinder.

4 Sintering

4.1 Micromechanical model

Several authors have developed mechanistic models for the different stages of the sintering process,[11–13] formulating evolution equations for the state variables density, interparticle neck size, and grain size. Finite-element simulations of the sintering of ceramic or metal parts are mostly based on phenomenological sintering equations.[14,15] In the present paper, sintering is simulated using the two-dimensional micromechanical model developed by Riedel and Sun[14] which has been formulated as a user's material subroutine in ABAQUS. For details of the integration procedure, see Sun and Riedel.[16] The model assumes a hexagonal arrangement of circular grains and grain boundary diffusion is the dominant material transport mechanism, which is true for a wide range of ceramic materials, particularly for oxides. Strain rates are calculated from the linear constitutive equation

$$\dot{\varepsilon}_{ij} = \frac{\sigma'_{ij}}{2G} + \delta_{ij}\frac{\sigma_m - \sigma_s}{3K} \tag{4}$$

where σ' denotes the deviatoric stress tensor, σ_m the mean stress, and σ_s the sintering stress. G and K are the shear and bulk viscosities, δ_{ij} is the Kronecker symbol. Expressions for the variation of the viscosities and the sintering stress versus relative density are derived in[11] yielding

$$G = \frac{\sqrt{3}kT(1-\omega)^3 d^3}{48\Omega\delta D_b},\ G/K = \frac{3}{4}\left(\frac{1-D}{1-D_1}\right)^{\frac{m+1}{m+5/3}} \quad \text{and} \quad \sigma_s = \sigma_{s1}\left(\frac{1-D_1}{1-D}\right)^{\frac{1}{3m+5}} \tag{5}$$

Here, Ω is the atomic volume, δD_b is the grain boundary diffusion coefficient, k is Boltzmann's constant, T is absolute temperature, and d is the grain facet diameter. D denotes the relative density, σ_{s1} is the sintering stress at the reference density D_1, and m is an empirical parameter describing the shape of the pore-size distribution function. The voided area fraction of the grain boundary ω is related to the density by

$$\omega = 3^{3/4}\sqrt{\frac{1-D}{\pi f(\psi)}} \tag{6}$$

where $f(\psi)$ is a pore shape factor. ψ is the dihedral angle defined by $\cos\psi = \gamma_b/(2\gamma_s)$, where γ_s and γ_b are the specific energies of the surface and the grain boundary, respectively. While some of the parameters like Ω and δD_b can be found in the literature,[17] others remain to be measured or plausible values have to be assumed. The values used in the present simulation correspond to those compiled by the author. They were measured in sinter for-

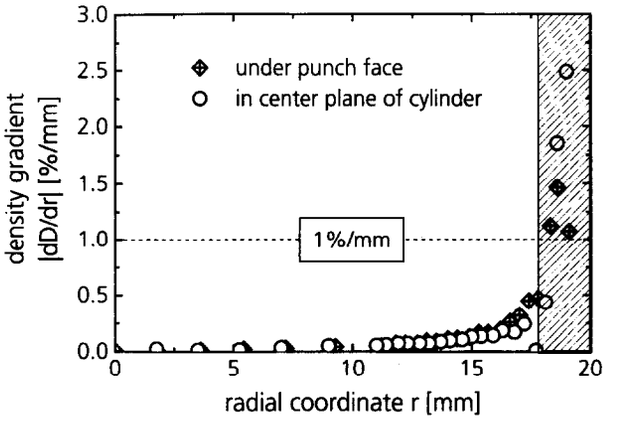

Fig. 6. Gradient of the relative density after pressing, evaluated for the centre lines of the upper surface of the cylinder and its center plane.

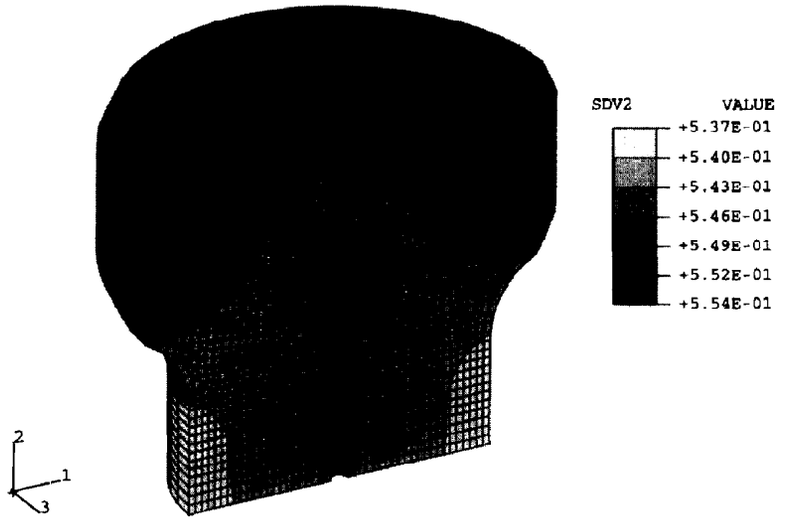

Fig. 7. Density distribution in the upper half of the machined part obtained by projection of the density distribution of the full cylinder onto the new geometry.

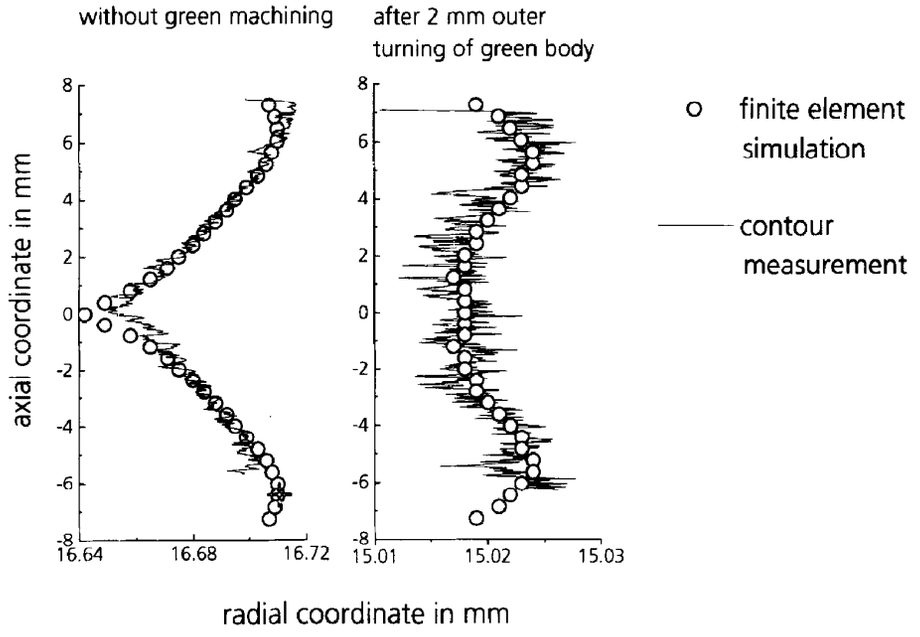

Fig. 8. Comparison of the predicted contour of the cylinder mantles after die pressing and sintering for the original and the machined cylinder with experimental results from profilometer measurements.

ging experiments with yttria-stabilized tetragonal zirconia in which cylindrical specimen are sintered under uniaxial load and the strain rates in axial and radial direction are measured during the densification process. The model parameters were fitted to reproduce these strain rates.[18] They should still lead to a good prediction of the shape distortion after sintering since the final shape is not much influenced by the choice of the parameters.

4.2 Finite-element simulation of the sintering

In order to verify the choice of parameters and the influence of green machining on the shape distortions of a cylinder, two simulations were performed with the same parameter values as above. In the first simulation, the cylinder was sintered without any machining while, for the second simulation, 2 mm of the outer surface were removed before the sintering simulation. Real cylinders were pressed and sintered at FRIATEC AG and machined at the Fraunhofer-Institute for Production Technology, Aachen, Germany. The shape distortions after sintering can easily be obtained by profilometer measurements.

Figure 8 shows the good agreement between measured and predicted contour of the cylinder mantle for the original and the green machined part. Also obvious is the influence of green machining, resulting in less than 10 μm difference between maximum and minimum radius for the machined part while the difference amounts to about 70 μm in the unmachined case.

As an application on real parts, a sintering simulation of the ceramic sensor in Fig. 7 is

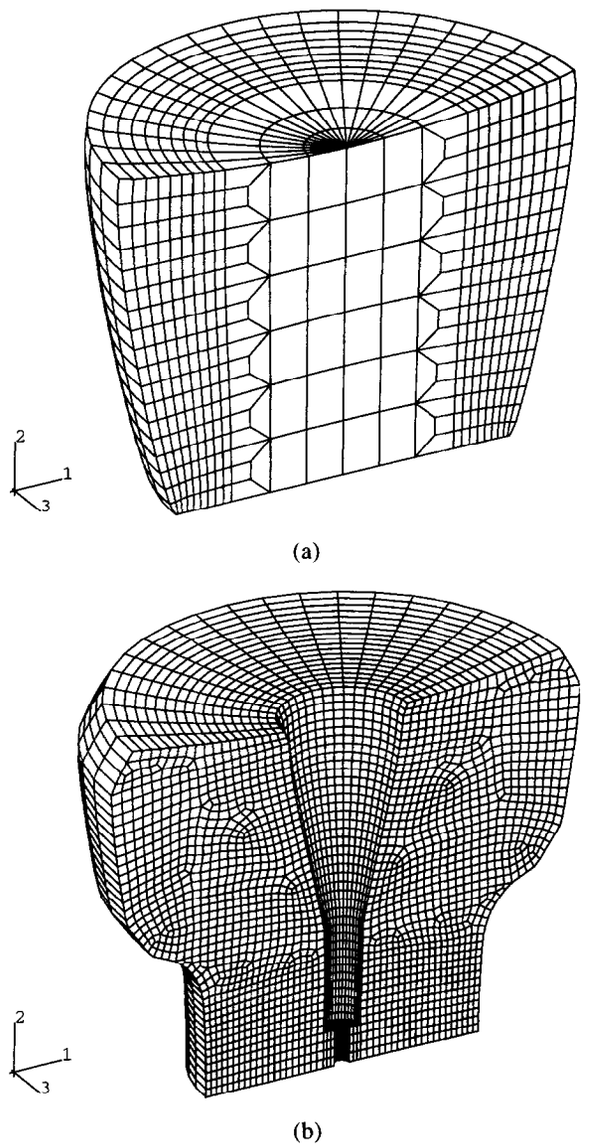

Fig. 9. Shape distortions of the machined part of Fig. 7 after sintering compared to those of the sintered cylinder of Fig. 5.

performed with the same set of parameters. Since regions of high density shrink less than regions of low density, shape distortions occur as shown in Fig. 9. The displacements are magnified by a factor of 5 in order to make the distortions clearly visible. The shape change of the machined part can be compared to the distorted geometry of the full cylinder after sintering. The regions near the cylinder walls contribute strongly to the change in geometry leading to a more pronounced distortion compared to the machined component.

5 Conclusion

The implementation of constitutive models for pressing and sintering into a general purpose finite-element program allows to calculate the density distribution of the green body and the shape distortion of the dense part. The exact determination of the model parameters for a specific powder requires large-scale experimental effort including triaxial presses as well as sinter-forging equipment. The extraction of the model parameters from the measured data is not straightforward. Nevertheless, good results can be obtained by a sensible estimation of most parameters combined with literature values and results of uniaxial pressing experiments which can easily be realized.

A careful analysis of the calculated density distribution of the pressed part provides the manufacturer with detailed information about problematic areas in the green body where high density gradients can occur. An optimization of the pressing tools as well as a modification of the machining can be achieved. Simulation of the sintering process not only yields the total shrinkage but also the shape distortions after densification. The calculated final geometry of the dense part can be compared to the tolerance criteria set up by the user, insuring product quality. Finally, the time between the design of a ceramic part and the final layout of the pressing tools and the sintering conditions can both be shortened and estimated more precisely in advance.

Acknowledgements

The author gratefully acknowledges financial support from the Bundesministerium für Bildung, Wissenschaft, Forschung und Technologie (BMBF) under contract 03M 2112A.

References

1. Helle, A. S., Easterling, K. E. and Ashby, M. F, *Acta metall.*, 1985, **33**, 2163–2174.
2. Fleck, N. A., Kuhn, L. T. and McMeeking, R. M, *Journal of Mech. Phys. Solids*, 1992, **40**, 1139–1162.
3. Fleck, N. A., *Journal of Mech. Phys. Solids*, 1995, **43**, 1409–1431.
4. Armstrong, S., Godby, V., Shankar Rachadonder, V. B., Cheng, S. and McCabe, T. J., In *Advances in powder metallurgy and particulate materials*, ed A. Lawly and A. Swanson, Vol. 3. Metal Powder Industries, Princeton, N.J., 1993, pp. 165–173.
5. Bortzmeyer, D., *Powder Technol.*, 1992, **70**, 131–139.
6. Nakagawa, T. and Nohara, A. In *Computer aided innovation of new materials*, ed. M. Doyama, T. Suzuki, J. Kihara and R. Yamamoto. Elsevier Science Publishers B. V., North Holland, 1991.
7. *ABAQUS Theory Manual*, Version 5.4, Hibbitt, Karlsson and Sorensen, Inc., Rhode Island, 1994.
8. Meyer, D., PhD thesis, University of Karlsruhe, Germany, 1994.
9. McMeeking, R. M. and Kuhn, L. T., *Acta metall. mater.*, 1992, **40**, 961–969.
10. Ernst, E., Axiale Preßvorgänge in der Pulvermetallurgie. *VDI Forschungsberichte*, **2**, (259), Verein Deutscher Ingenieure, Düsseldorf, 1992.

11. Gillia, O, Bouvard, D., Doremus, P. and Imbauld, D. In *Advances in hard materials production*, Euro PM 96, Stockholm, 1996, pp. 61–68.
12. Bordia, R. K. and Scherer, G. W., *Acta metall.*, 1988, **36**, 2393–2397.
13. Riedel, H., Zipse, H. and Svoboda, J., *Acta metall. mater.*, 1994, **42**, 435–443, 445–452.
14. Riedel, H. and Sun, D.-Z. In *Numerical Methods in Industrial Forming Processes*, NUMIFORM '92 , ed J.-L Chenot, R. D. Wood and O. C. Zienkiewicz. A. A. Balkema, Rotterdam, 1992, pp. 883–886.
15. Mori, K. In *Numerical Methods in Industrial Forming Processes*, NUMIFORM '92, ed J.-L Chenot, R. D. Wood and O. C. Zienkiewicz. A. A. Balkema, Rotterdam, 1992, pp. 69–78.
16. Sun, D.-Z. and Riedel, H. In *Simulation of Materials Processing: Theory, Methods and Applications*, NUMIFORM '95, ed. S.-F. Shen and P. Dawson. A. A. Balkema, Rotterdam, 1995, pp. 881–886.
17. Helle, A. S., Licentiate thesis, University of Lulea, Sweden, 1986.
18. Zipse, H. and Riedel, H. In *Ceramic Processing Science and Technology*, ed. H. Hausner, G. L. Messing and S-I. Hirano. The American Ceramic Society, Westerville, 1995.